# Novel FRF-based fast modal testing of multi-storey CLT building in operation using wirelessly synchronised data loggers

Wai Kei Ao[a,*], Aleksandar Pavic[b,**], Blaž Kurent[c,], Fernando Perez[d,]

[a]*The Hong Kong Polytechnic University, Civil and Environmental Engineering, Hung Hom, Kowloon, Hong Kong*
[b]*University of Exeter, Vibration Engineering Section, College of Engineering, Mathematics and Physical Sciences, North Park Road, Exeter EX4 4QF, U.K.*
[c]*University of Ljubljana, Faculty of Civil and Geodetic Engineering, Jamova cesta 2, 1001 Ljubljana*
[d]*Smith and Wallwork Ltd, 50 St Andrews Street Cambridge, CB2 3AH, UK*

**Abstract**

This paper presents a novel input-output frequency-response function (FRF) based field modal testing (MT) of an operational and fully occupied tallest cross-laminated timber (CLT) building in the U.K. A custom-built MT system and testing protocol were developed to facilitate exceptionally fast field testing work lasting only 10 h, including all instrumentation and field testing work.

This yielded eight fundamental and higher-order modes of vibration with natural frequencies up to 12 Hz. The higher order modes are normally not possible to measure well enough using the standard output-only operational modal analysis (OMA). An FE model was developed prior to the testing to assure quality and facilitate the fast testing process. The FE model, based on the best engineering judgement, proved to be able to predict very well the key features of the test building. This includes close matching and correct clustering of the FE-calculated and MT-estimated natural frequencies, as well as a very reasonable prediction of the static stiffness at the top of the building. The in-situ measured horizontal static stiffness at the top of the CLT building is a considerable benefit of the field FRF measurements and is not possible in the standard OMA. It was shown that the preliminary best practice FE model was over-predicting the static stiffness in the two orthogonal directions by only up to 22 % of the measured values.

*Corresponding author
**Principal corresponding author
*Email addresses:* waikei.ao@polyu.edu.hk (Wai Kei Ao), a.pavic@exeter.ac.uk (Aleksandar Pavic), blaz.kurent@fgg.uni-lj.si (Blaž Kurent), fernando.perez@smithandwallwork.com (Fernando Perez)

Curve-fitting of the good quality FRF data yielded damping ratio values for the higher order modes of vibration, typically above 3 %. This is quite high for a full-scale multi-storey residential building.

*Keywords:*
modal testing, full-scale, CLT building, frequency response function, OCXO-based synchronised data loggers

## 1. Introduction

Medium to very tall high-rise buildings dominate the skylines of many cities in the world, which decided to go 'up' rather than 'out' to cope with transportation and other challenges facing their growing population. Vibration serviceability due to wind-induced lateral sway has become the de-facto governing design criterion for high-rise buildings above 50 m, dictating the size, shape and therefore cost of such structures [1]. Damping ratios and natural frequencies of all modes of vibration that can be excited by wind are the key modal parameters which are used in design to size the structure and predict wind-induced sway vibrations of tall buildings in service.

However, long-term practice is showing that damping and natural frequencies of tall buildings are also quite unreliable parameters to assume in design. Underestimation of the fundamental natural frequency of up to 50 % by the finite element model (FEM) relative to its experimental counterpart is common ([2]). The situation with damping ratios is similar or worse due to even greater uncertainties in the values of modal damping ratios measured in as-built buildings. This is because the natural frequencies and damping ratios in as-built tall building structures are fundamentally non-linear and amplitude-dependent ([2]). Therefore, standard output-only ambient vibration testing (AVT), also known as ambient vibration survey (AVS) or operational modal analysis (OMA), methods for their estimation - based only on the measured responses to unmeasured ambient excitation which vary with time - are naturally producing estimates of modal parameters which vary considerably from one block of data to another ([3]; [4]).

An input-output modal testing (MT), or experimental modal analysis (EMA), where both the excitation force and the corresponding dynamic response are measured simultaneously with the aim of experimentally estimating the structure's frequency response function (FRF) is a much more powerful tool to deal with structural non-linearities and uncertain modal parameters such as the natural frequency and damping. For decades MT has traditionally dominated aerospace and automotive sectors, whereas AVT has been very much used in experimental dynamic testing of large civil engineering structures. This even though AVT has, by its very nature and due to its underpinning assumptions ([5]; [4]), rather inferior performance as to its quality of modal parameters relative to MT.

The key reason for this situation is practical difficulties in exciting a massive full-scale tall building in a noisy open-space environment with a measurable force causing measurable response without damaging the building at the point of excitation. Even if this first problem is, overcome then the next is the logistical challenge of measuring such responses simultaneously throughout the building. These are needed to estimate experimentally mode shapes to complete the set of four modal properties: natural frequencies, modal damping ratios, modal masses, and mode shapes. Finally, the last problem is to do it extremely fast on a typically operational building, which is relevant and needed for serviceability investigations, to avoid disruption. Hence, MT results based on the experimentally measured FRFs across a wide range of frequencies, fast and in operational multi-storey buildings practically do not exist in the literature.

This paper addresses this gap and describes a novel FRF-based MT of a multi-storey residential building in operation to measure its important sway modes. The building is the tallest timber building in the UK constructed in 2017 in Glasgow in an area known as Yoker. The Yoker building is a seven-storey building containing 42 occupied flats made entirely of cross-laminated timber panels. To the best knowledge of the authors, this is the first ever attempt to conduct an FRF-based MT on an occupied multi-storey residential building.

The testing was conducted using a set of synchronously operating electrodynamic shakers and wirelessly synchronised oven-controlled crystal oscillator (OCXO)-based data logger in conjunction with high-precision accelerometers for simultaneous force and response measurements ([6]). The key novelty of this MT system is that it makes no use of cables or radio waves to connect the response accelerometers throughout the building simultaneously with the multi-channel data acquisition system. However, it still provides a perfect synchronous measurement of a practically unlimited number of force and response channels. This new FRF-based modal testing process will be described in detail in this paper using the Yoker building as a case study.

After the introduction, Section 2 describes the test structure. Section

3 presents finite element (FE) modelling and results of the modal analysis. Following best practice in FRF-based modal testing ([7]), these preliminary results informed the set up of the modal testing apparatus and the corresponding testing protocol, which are presented in Section 4. Section 5 describes the results of the modal testing and compares them with the preliminary FE modelling results. Finally, Section 7 presents conclusions.

## 2. Structural description

Figure 1 is two photos of the Yoker building made in November 2019.

Figure 1: Two views of the Yoker building.

The main load-bearing super-structure of the building is made entirely of CLT panels: horizontal for floors and vertical for the internal walls, including the lift shaft and façade. Only the foundations and ground slab are made of reinforced concrete, as appropriate.

The building has a T-shaped plan and is divided into North and South wings, as shown in Figure 2. The North wing is connected to the Southern wing only through the communal corridor/lobby where the stairwell and lift are located. The lightweight cladding was used for the façade. The height of the building is approximately 22 m. Figure 3 shows key structural details and CLT connections of the Yoker building.

The total mass of the building is approximately 1,300 tonnes.

## 3. FE modelling in preparation for modal testing

Following good practice and to quality assure full-scale modal testing, a representative finite element (FE) model was developed ([7]) based on the best engineering judgement using ANSYS software ([8]).

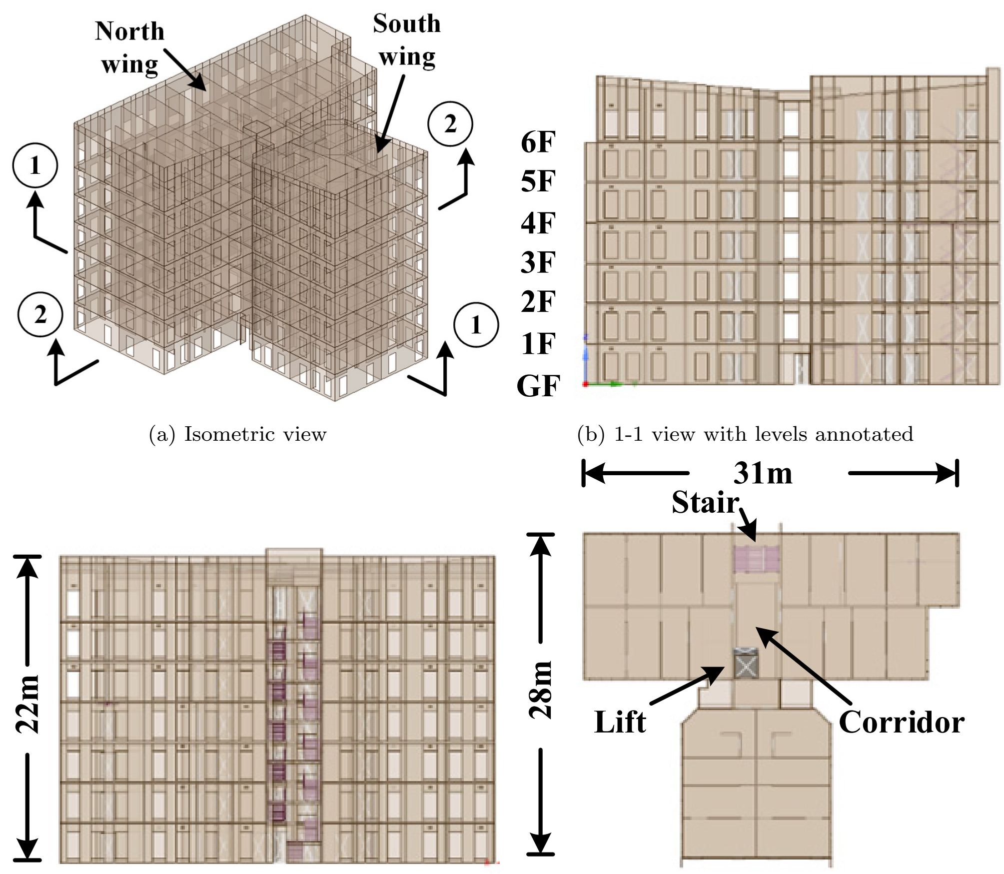


(a) Isometric view

(b) 1-1 view with levels annotated

(c) 2-2 view

(d) Top view

Figure 2: Isometric, side and plan views of the Yoker building.

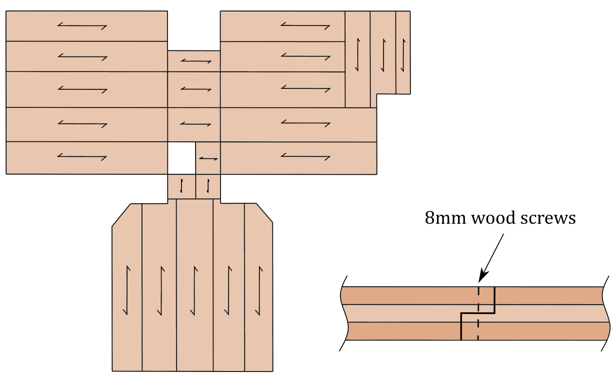


(a) Typical floor plan with CLT panels orientations and typical connection between the panels. This particular plan is for $4^{th}$ to $6^{th}$ storey

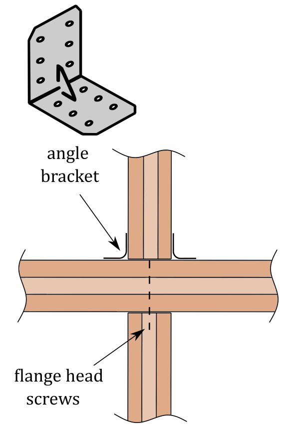


(b) Typical wall-slab joint

Figure 3: Key structural details of the Yoker CLT building (after [8]).

The CLT panels were modelled using the SHELL181 ANSYS element, and these elements accounted for 515 t of the total mass of the building. Then, the mass of well-defined non-structural elements (partitions, etc.) was 685 t, and the 'uncertain' mass of other non-structural elements, such as furniture, doors, windows and services, was estimated at 70 t. The non-structural mass was distributed throughout the building based on its location by increasing the mass of the relevant structural elements, as appropriate, using SURF154 elements. Five types of CLT panels were used with three or five layers with total thickness varying from 100 to 200 mm. Key material properties of timber were assumed based on the data from its producer Stora Enso ([9]), as follows:

- Elastic moduli $E_0 = 12,000$ MPa and $E_{90} = 370$ MPa;
- Shear moduli: $G_{0,90} = 460$ MPa and $G_{90,90} = 50$ MPa;
- CLT density: $\rho = 470$ kg/m$^3$;
- Poisson's ratio is $\nu_{0,90} = 0.3$

The $_0$ and $_{90}$ sub-scripts represent the timber layer's orientation angle in the CLT panel. The wall-to-wall and wall-to-floor CLT connections were assumed to be rigid. Further details of this initial FE model are presented elsewhere ([8]).

Figure 4 shows the considerable level of the FE modelling detail and the meshing size adopted.

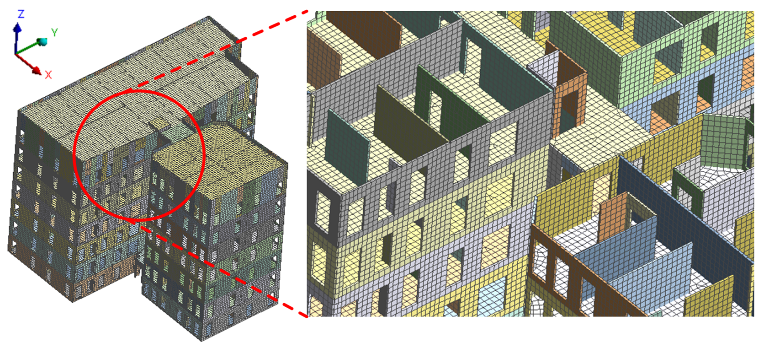


Figure 4: The Yoker building FE model and its meshing detail.

Figure 5 shows the eleven FE-calculated modes of vibration, which were used to inform the modal testing. There are two clear clusters: around 3-4 Hz and 8-12 Hz. This kind of clustering is therefore expected to be observed in the experimental FRF data during their initial in-situ quality check.

## 4. FRF-based modal testing of occupied full-scale building

As previously mentioned, FRF-based modal testing of an occupied multi-storey residential building is an ultimate challenge in vibration serviceability research on fully operational buildings. Being input-output based, it provides the best quality experimental modal data (natural frequencies, mode shapes, modal damping, modal mass) for a fully operational residential building. As opposed to partially finished buildings, which are normally available for and used for AVT in the past, modal data from occupied residential buildings based on experimental FRFs over a full range 0-12 Hz is virtually non-existing.

### *4.1. Modal testing and FRF data acquisition specifications*

The key reason for this situation is the tremendous practical and logistical problems to:

1. gain access to an occupied building and carry out the tests quickly and without disturbing the building occupants,

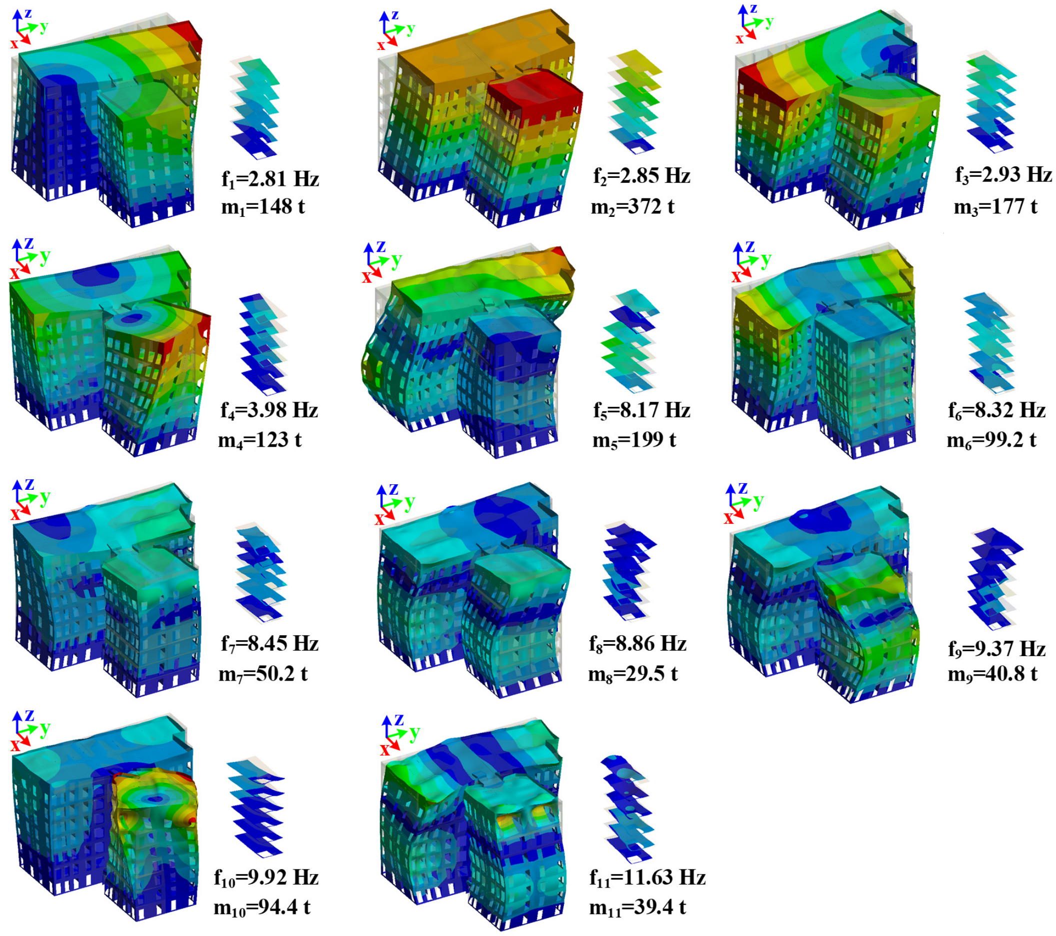


Figure 5: Natural frequencies and mode shapes of the first 11 modes of the Yoker building.

2. provide and operate sufficient measurable excitation, typically at the top of the building, and

3. record continuously and simultaneously the excitation force and the corresponding vibration response at multiple levels of the building, which is needed to measure the mode shapes.

Therefore, the following specifications were developed for this modal testing:

- To address problem 1, the testing had to be finished in a single day using only existing facilities within the building (staircases, an elevator, normal mains 240 V power supply, single parking space in front of the building, etc.).

- To address problem 2, a set of portable horizontal shakers was employed, which could be moved manually and transported to the top of the building using the existing elevator in the building. The shakers were selected based on the FE calculated natural frequencies and modal masses calculated using a unity-scaled mode shapes (Figure 5) so that they had sufficient force to excite the whole 1300-tonne building laterally. This was done in conjunction with the ultra-sensitive accelerometers distributed throughout the building, which could measure the resulting building sway response.

- To address problem 3, there was a need to eliminate wires between the accelerometers throughout the building and the multi-channel force and response data acquisition system at the top of the building, placed next to the exciters. Therefore, a novel wireless data acquisition system was developed able to simultaneously record multi-channel force and acceleration digital data in the time domain. Considering that radio connections seldom work well in occupied buildings, a set of very precisely synchronised data loggers was developed. This was based on an oven-controlled crystal oscillator (OCXO) synchronisation enabling less than a micro-second time shift between the physical loggers, which was more than enough accuracy for FRF measurements of a low-frequency civil engineering structure. Figure 6 shows the hardware of the OXCO-based data logger. This device, developed in the laboratory of the Vibration Engineering Section (VES) at the University of Exeter is described in detail elsewhere ([10]; [6]).

OCXO-based data loggers could distinguish between 'master' and 'slave' during application. As a master clock/ticks, only one distributed data logger is initially chosen. The chosen 'master' data logger must then be connected to the DC/AC power in order to activate. A beep sound is announced when the master data logger and clock/ticks are successfully activated. The remaining 'slave' data loggers and the local clock/ticks are then separately powered on and activated using the same procedure. The next step is to synchronise the 'local' units. The correlated graphical block diagram programming of Labview is demonstrated in Figure 7a. The primary concept is to convert the binary 'master' clock ticks into an analogue number and subtract the 'slave' clock to calculate the difference. Then, the 'master' clock/ticks could be added/overwritten the difference to other 'slave' clock/ticks. This action is physically done using a BNC cable to connect the 'master' data logger output port with each of the 'slave' units' input port, as shown in Figure 7b.

The OCXO-based data logger also includes on-site visualised data recording and time synchronisation operations, as shown in Figure 8. A 'master' clock/ticks (see Figure 8a) was counting the number beyond the others. Figure 8b shows one of the slave clocks/ticks. It can be seen that the 'slave' OXCO count/ticks was lower than the 'master' OXCO count/ticks since the first 300000 sample points were recorded before the 'master' OCXO added or overwrote any ticks. After that, the physical BNC link from the 'master' to the 'slave' clock/ticks, the 'slave' unit could be overwritten at the precise synchronised point, resulting in an OCXO count jumping, as shown in Figure 8b insert plot. This jumping might serve as a time synchronisation indicator, making it convenience for the test crews to observe the time synchronisation process in real-time. The benefit only took a few seconds for each 'slave' unit and was conducted once at the start of the test.

### *4.2. Modal testing test grid throughout building*

To avoid disturbing the building occupants, the key instrumentations (shakers and accelerometers) were placed only in the building corridor(s) as no permission was given to enter and instrument any of the 6 flats on each floor level. Therefore, there are no test locations at the far ends of the North and South wings of the building, which would be logical choices to pick up more twisting modes (Figure 2). Figure 9 shows the modal testing grid and

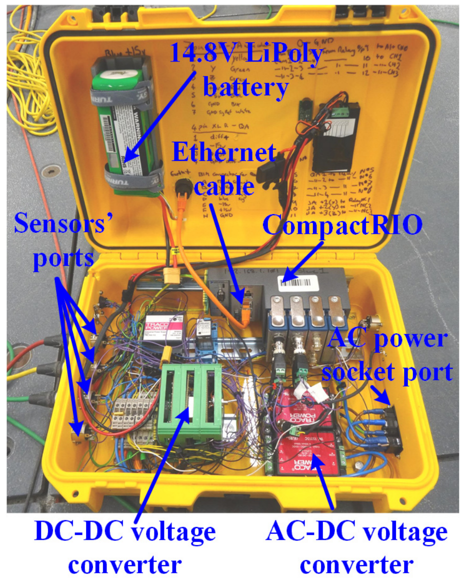


Figure 6: OXCO-based data logger featuring CompactRIO data acquisition hardware (after [10];[6]).

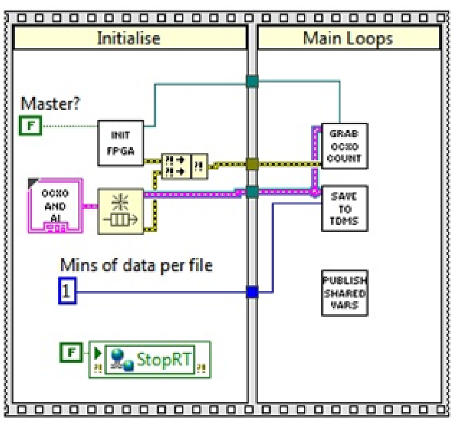


(a) LabVIEW real time block diagram of the CompactRIO-9064

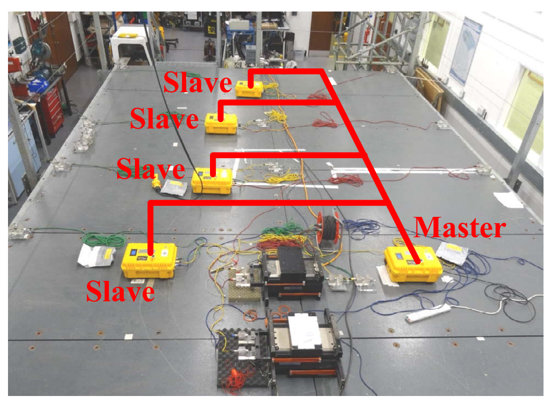


(b) Time synchonisation: connecting a 'master' OCXO to 'local' OCXO units

Figure 7: Master and slave OCXO units time synchonisation (after [6]).

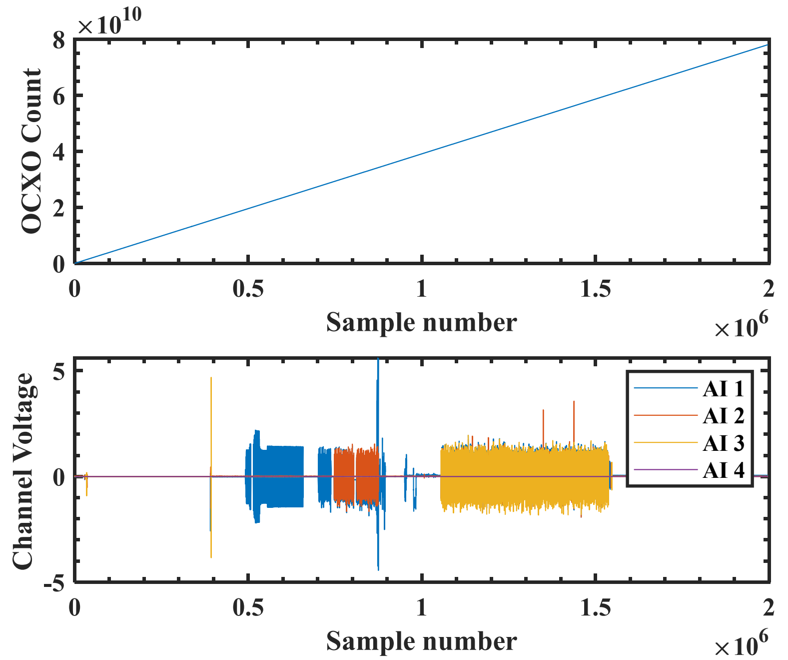


(a) Master OCXO

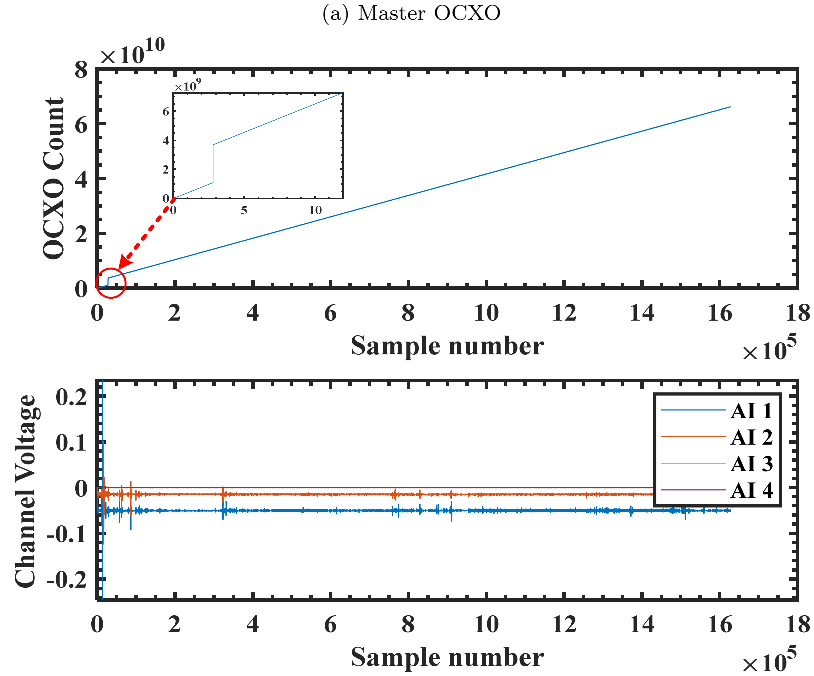


(b) Slave OCXO

Figure 8: Demonstration of 'master' clock/ticks OCXO count adding/overwriting the 'slave' clock/ticks to achieve the time synchronisation process.

orientation of accelerometers adopted over the height of the building. Figure 10 shows the measurement points and locations on the plan of the typical floor levels.

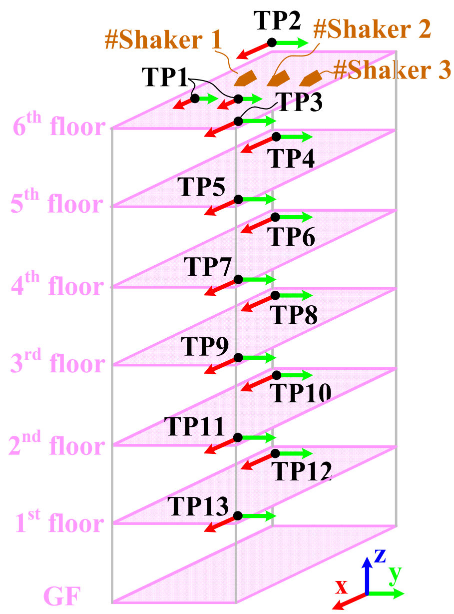


Figure 9: Test grid points were possible only within a rectangular corridor between the six flats shown in Figure 10.

Clearly, with such a limited test grid, a potential issue could have been with an insufficient spatial resolution to describe the mode shapes sufficiently well. To check this, an auto Modal Assurance Criterion (Auto-MAC) [7] was calculated using the selected test points and degrees of freedom (DOF) in the FE-calculated mode shapes (Figure 11). The limited test grid, in principle, has sufficient resolution to describe the eleven identified modes of vibration (see parts of the mode shapes corresponding just to corridors in Figure 5). The only exception is modes 2 and 4, which could be swapped and misinterpreted due to their high AutoMAC value of 0.8. Figure 12a shows a setup for the FRF point mobility measurement at the top floor and Figure 12b shows a typical response-only setup at one of the lower levels in the building. It is noted that Figure 13 demonstrates the horizontal alignment and setup details for several shakers. The self-weight plus reaction mass and friction-grasping support frame may successfully stabilise the shaker. Additionally, the proper input force management is required to guarantee that the driving

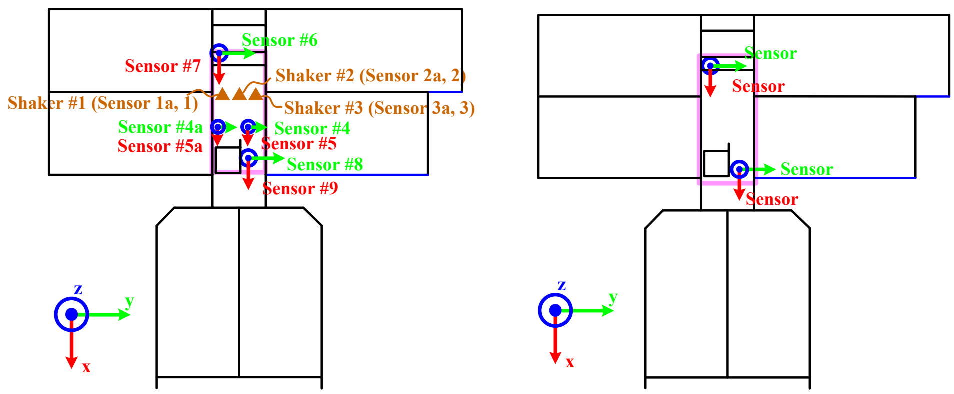


(a) $6^{th}$ floor instrumentation

(b) $1^{st}$ floor to $5^{th}$ floor instrumentation

Figure 10: Modal testing instrumentation shown in floor plans.

voltage results in steady shaker operation. After that, the shaker will not be requested to add any extra consolidated mounting. This semi-mounted method could be less disruptive, less intrusive, and flexible to the occupied properties, such that there is no need to request new drilling holes and use an invasive mounting strategy. This is another crucial justification for adopting these settings. The input voltage trail (from 0.5 to 1.75 V) for testing the ideal input voltage to drive the shaker is shown in Figure 14. The finalised input voltage was chosen at 1.5 V to compromise functionality and safety after on-site visualisation of the shaker stroke, force output level, robustness, and structure-shaker connecting stability. Consequently, the shaker and structure did not require any special connections or stingers.

### *4.3. Modal testing data flow*

A key limitation of the OXCO-based data loggers is that they could not be live-monitored during the modal testing. Although they recorded simultaneously all the time-domain modal testing data, that was done 'blindly' during the testing as the recorded data were available for visualisation and post-processing only after the testing.

However, a good practice in MT ([7]) and a key part of the quality assurance system in VES when doing FRF-based field modal testing is to - at least - visually monitor the formation of the point-accelerance FRF. This FRF is crucial for the curve-fitting quality ([7]). In noisy, open-space environments experimental measurement of FRFs requires averaging of multiple data blocks to remove extraneous noise on response channels ([7]). Greater

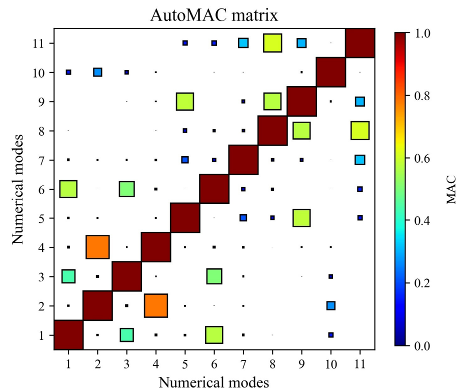


Figure 11: AutoMAC calculation corresponding to first 11 modes of vibration based on the pre-test FE model.

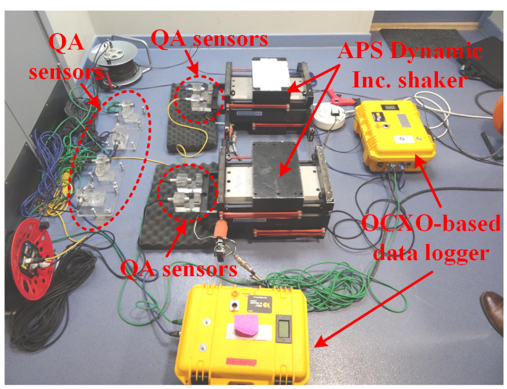


(a) Excitation and response measurement setup at top floor

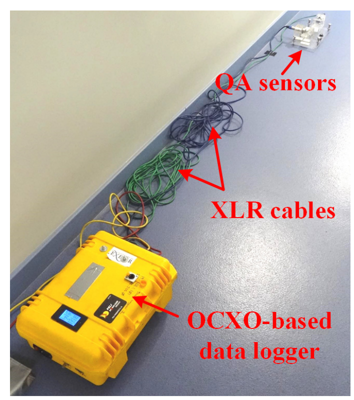


(b) Typical response-only point measurement setup

Figure 12: Modal testing instrumentation featuring OCXO-based data loggers: (a) measurement of the excitation using three APS400 electrodynamic shakers (the photo shows only two shakers) by utilising QA 750 sensors mounted on the shakers to measure the acceleration of the moving shaker armature of known mass and on the floor to measure floor accelerations; (b) typical QA 750 sensors setup to measure floor horizontal accelerations on one of the lower floor levels.

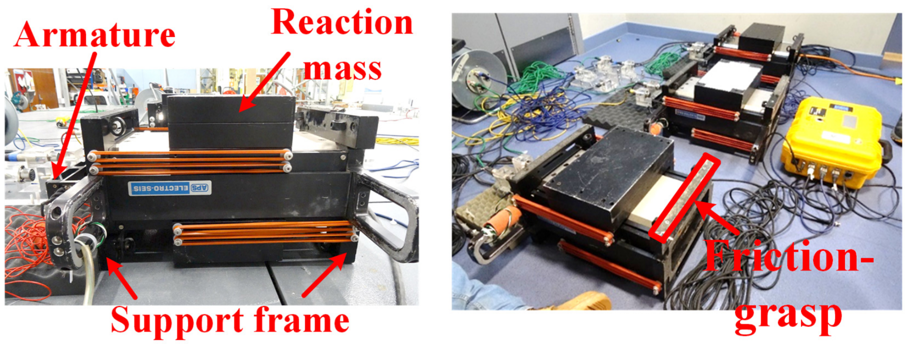


Figure 13: The configuration detail of the APS shaker horizontal setup and friction-grasping mount in the laboratory and field testing.

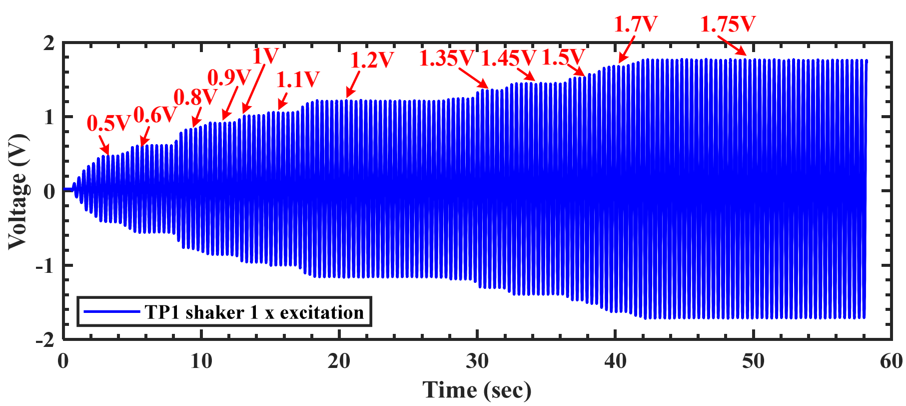


Figure 14: Different trail input voltage evaluation for the shaker.

extraneous excitation (e.g. due to wind) requires more averages to remove it and hence longer data acquisition. Therefore, the number of averages depends on the level of that extraneous noise which is never known in advance of the test. By live monitoring how the point-accelerance FRF 'settles' and stabilises with the increasing number of averages, the overall data acquisition time can be set. This is of crucial importance in severely time-limited exercises of this type whereby a minimum number of averages is needed to shorten the data acquisition time while still producing a usable set of FRFs. Figure 15 shows a point accelerance FRF measured on the Yoker building after only 1 average using 80 s of data and after 100 averages using over 30 minutes of data with 75 % of data block overlapping. The difference between them is remarkable, indicating the importance of the monitoring of the FRF formation during the MT.

To address this quality assurance problem, a standard 'wired' spectrum analyser (SA) was used to monitor only the formation of the point-accelerance FRF corresponding to the shaker excitation and structural response at the top of the building. This was done using a separate and independent set of 'wired' transducers measuring nominally identical data as the transducers feeding data to the OXCO data logger. These wired transducers were positioned very close to the data acquisition centre to reduce the length of the standard wires, as shown in Figure 16. The spectrum analyser was also used to generate random signals for the shakers.

Figure 17 shows the data flow enabling 'dual' measurement of the point mobility FRF for on-site immediate visual inspection and off-site post-processing.

### *4.4. Modal testing instrumentation*

Apart from the already described OXCO-based data logger (Figure 6), the spectrum analyser used was the 20-channel Data Physics DP730 in conjunction with a 10-channel signal conditioner (Figure 18a) for Honeywell QA 750 uniaxial force-balanced accelerometers ([12]). Also, Japan Aviation Electronics (JAE) JA-70SA tri-axial MEM accelerometers ([13]) were used to measure the structural response. The two types of accelerometers used are shown in Figure 18b.

Figure 18a also shows a compact and portable instrumentation rack featuring amplifiers for the three APS shakers used as well as the laptops for driving the system and immediate point accelerance FRF data (instantaneously available from the spectrum analyser) processing, part of the VES QA system for field FRF measurements. Namely, considering very short

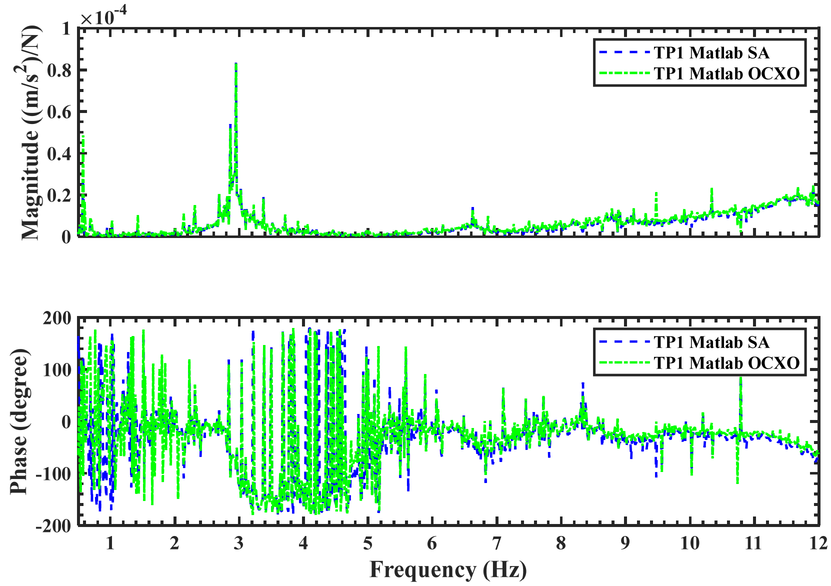


(a) Point accelerance FRF measurement

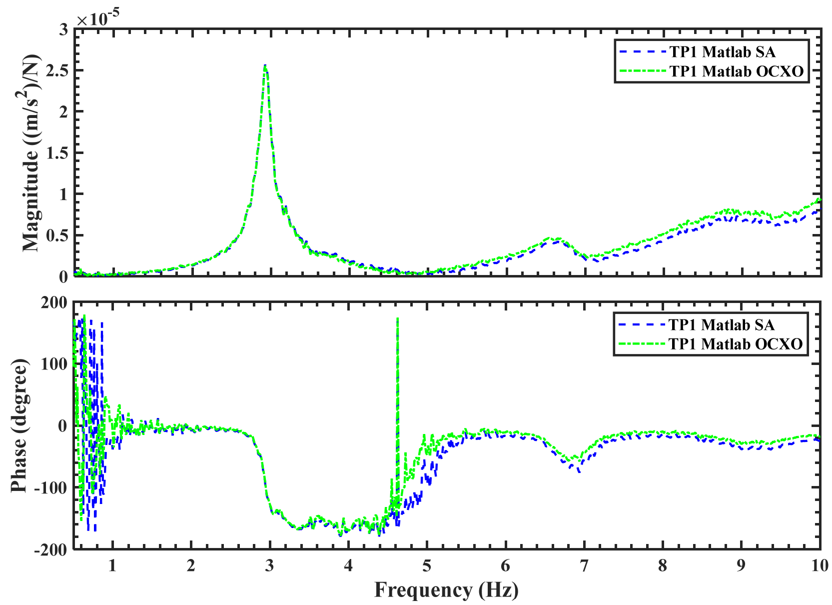


(b) Point accelerance FRF measurement

Figure 15: Point accelerance FRF measurement in the North-South (X-direction, Figure 9) at $6^{th}$ floor. (a) corresponds to one averages, and (b) corresponded to 100 averages which is the final number of averages adopted for the measurements. Total data acquisition time to be able to do 100 averages with 75 % overlapping and Hanning windowing of data blocks was over 1800 s.

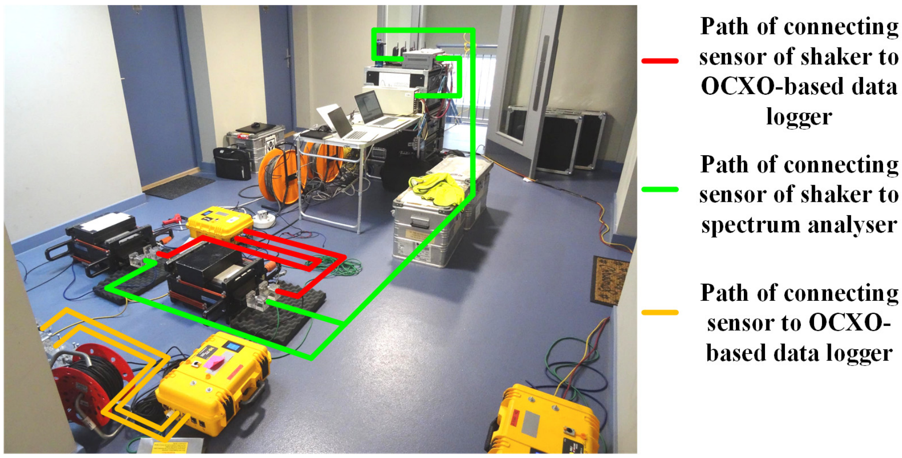


Figure 16: Dual 'wired' and 'wireless' FRF data acquisition system at the top of the building. It can be seen that the shakers have two accelerometers each mounted to measure the same acceleration of the moving armature of the known mass i.e., the excitation force. For each shaker, signal from one accelerometer is wired directly into the spectrum analyser (green lines) while the other accelerometer is connected to the yellow OCXO box (red line). The two accelerometers measure nominally the same acceleration.

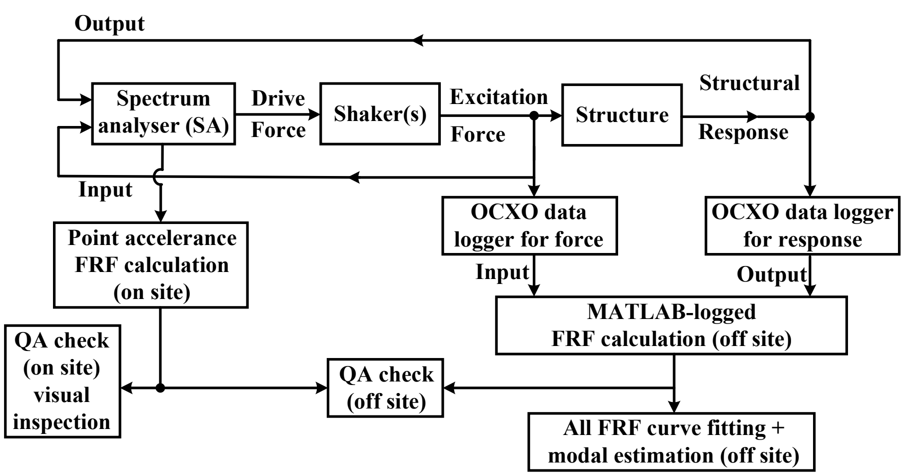


Figure 17: Flow of data in the 'dual' wired and wireless FRF data acquisition system (after [11])

time scales to run the tests and often inability to repeat the test at a later date if something goes wrong and is not discovered immediately, part of the QA process used requires immediate processing of any of the in-situ available FRFs to check if they could be processible producing meaningful modal estimation. Further information on the adopted instrumentation and methodology used is available elsewhere ([6]).

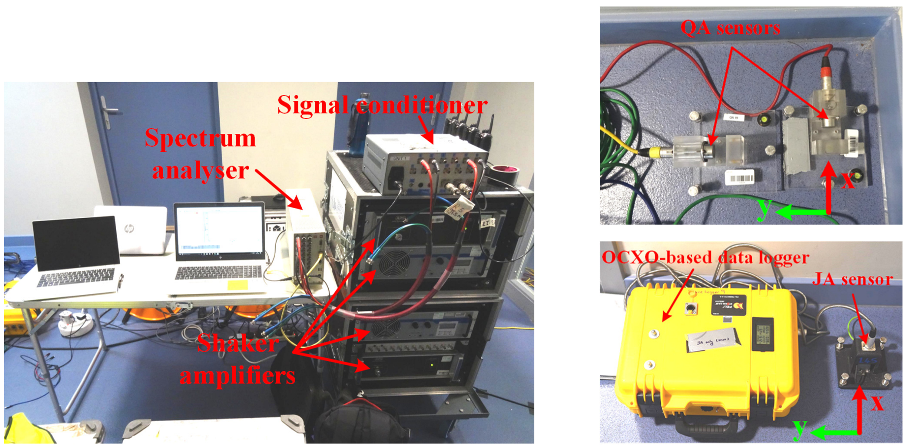


(a) Data acquisition system

(b) Accelerometers

Figure 18: (a) Data acquisition centre and (b) Uniaxial QA 750 and tri-axial JA-70SA accelerometers used and their alignment in the X and Y directions of the CLT floor of the Yoker building.

### *4.5. Modal testing logistics and timing*

After six months of preparations and practising fast deployment, setting up, data acquisition, checking and packing of the modal testing equipment, the FRF-based modal testing took place on $21^{st}$, January 2020. The test team had four members, and the whole of the test equipment was packed in a single van occupying only a single car park space at the Yoker building (Figure 19). The modal testing was done in only 10 hours. The test team arrived at 8 a.m., unloaded and deployed the equipment, performed modal testing, packed and loaded the equipment back into the van. The team left the site by 6 p.m. on the same day.

### *4.6. Modal testing raw data and their checks*

As the speed of the modal testing process was of paramount importance, a broadband random excitation 0-12 Hz was applied through three synchron-


Figure 19: A long wheelbase van with equipment packed and ready to be deployed. The total weight of the equipment was less than 1 tonne and individual pieces were less than 50 kg each enabling safe and easy manual handling by two people.

ously running shakers, first in the X-direction (Figure 20a) and then in the Y-direction (Figure 20b). This was done via a random signal generated by the DP730 spectrum analyser which was simply split three ways so that three identical analogue random signals were fed to the amplifiers of the three shakers generating their driving voltage.


(a) X-direction excitation


(b) Y-direction excitation

Figure 20: Synchronous random excitation by three horizontal APS400 shakers: (a) in the X-direction and (b) in the Y-direction.

#### *4.6.1. Checking of synchronously running shakers*

Multiple shakers had to be utilised in the test to provide a sufficient force level to excite the structure. The BNC channel T-splitter (see Figure 21) could be used at the spectrum analyser output port to diversify the input signal and drive each exciter to reach the performance of the single input, which could ensure the exciters were operating in phase. In other words, when the shakers receive out-of-phase input, they behave non-synchronised, which results in a time delay and amplitude deduction issues that lower the total force generation. The synchronised sinusoidal input time history evidence of shakers is shown in Figure 22. Each shaker input force measurement's forms under various resonant sinusoidal excitation frequencies had a constant amplitude and phase. The total force engagement was taking the sum of the shakers instead of averaging the value.

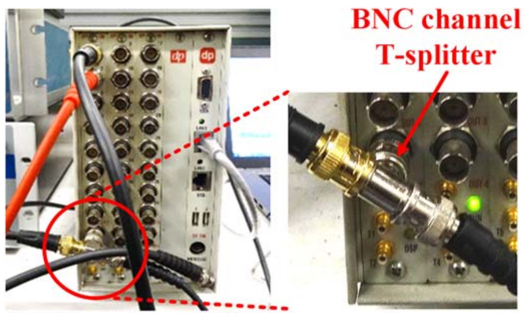


Figure 21: Spectrum analyser and BNC channel T-splitter of the single output port.

*4.6.2. Excitation in X-direction*

A single-input multiple-output (SIMO) FRF measurement and modal testing process was applied, with all three shakers assumed to generate a single random force exciting the building at its top and along a single degree of freedom (DOF) corresponding to the location and orientation of the shakers at TP1 (Figure 9). Although the shakers excited only one DOF (either X- or Y- direction) at the time, the structural vibration responses were measured in both X- and Y- directions simultaneously over all floor levels. This resulted in a single column of the FRF matrix with a total of 26 elements, half of which corresponding to the X-direction and the remaining half to the Y-direction excitation at TP1 (Figure 9).

As previously mentioned, the shaker force was measured by measuring acceleration (using QA 750 accelerometers) of the shaker armature mass of 22.95 kg. Hence, Figure 23a shows the total force applied at TP1 in the X-direction and the corresponding acceleration responses in the X- direction (Figure 23b) and Y-direction (Figure 23c). The root mean square (RMS) of the random force signal was 500 N with occasional peaks just over 1 kN. As the random vibrations caused by the shakers were not perceptible by the test personnel at the top of the building or anywhere else within the building,

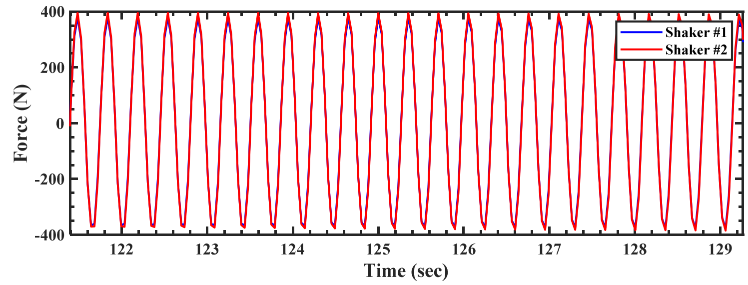


(a) Mode 1: $f_1 = 2.84$ Hz

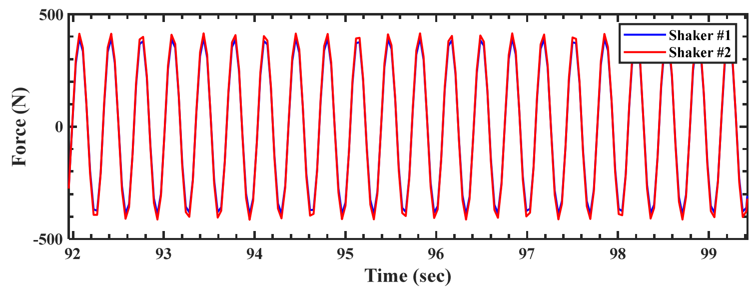


(b) Mode 2: $f_2 = 2.93$ Hz

Figure 22: Input force time history of each shaker representing to modes 1 and 2.

it was reassuring to see that the random accelerations in the X-direction at TP1 were considerably larger than in the Y-direction, as expected considering the mode shapes (Figure 5). This check was important to ascertain that the whole 1,300-tonne building was clearly responding to the shaker excitation in the X-direction in a logical manner in addition to any not measured extraneous excitation within and outside the building.

Using a 75 % overlap of individual data blocks lasting 80 s each, 100 averages, Hanning window were used to estimate the FRFs with the frequency resolution of 0.0125 Hz.

Based on these data acquisition and analysis parameters, Figure 15b shows FRF point accelerance in the X-direction at TP1 and Figure 24 shows FRF transfer accelerance between the X- and Y- directions at TP1. The transfer FRF magnitude has a considerably lower magnitude than the point FRF magnitudes, as expected, and it is also noisier due to worse signal-to-noise ratios. However, clear modes between 2 and 3 Hz are identifiably confirmed by clear phase shifts. After the modal test on the day, MATLAB was used to process data from the OXCO data loggers and the FRF plots in

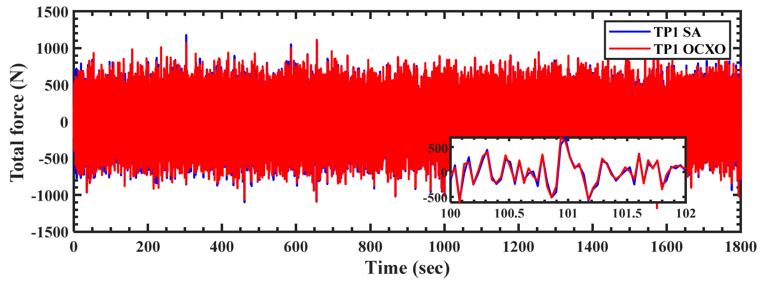


(a) Total random force in the X-direction

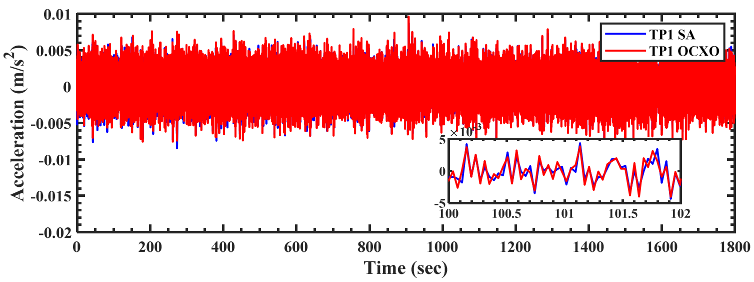


(b) Acceleration response in the X-direction

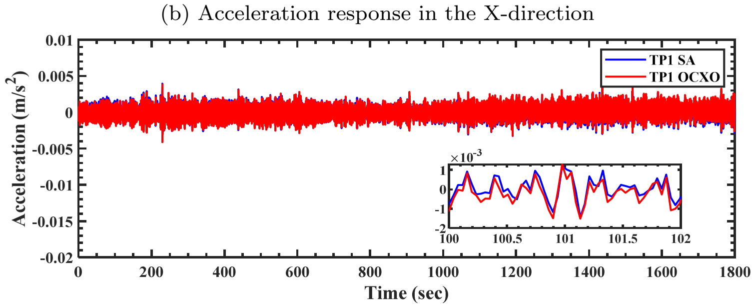


(c) Acceleration response in the Y-direction

Figure 23: (a) Total random excitation force in the X-direction applied by three APS400 shakers applied at TP1. The corresponding random response at TP1 in (b) the X-direction and (c) the Y-direction.

Figures 15 and 24 also demonstrate that the 'wireless' OCXO- and 'wired' SA-based data acquisition systems generate practically identical FRF data. This confirmed the ability of the OXCO-based system to generate good-quality FRF data.

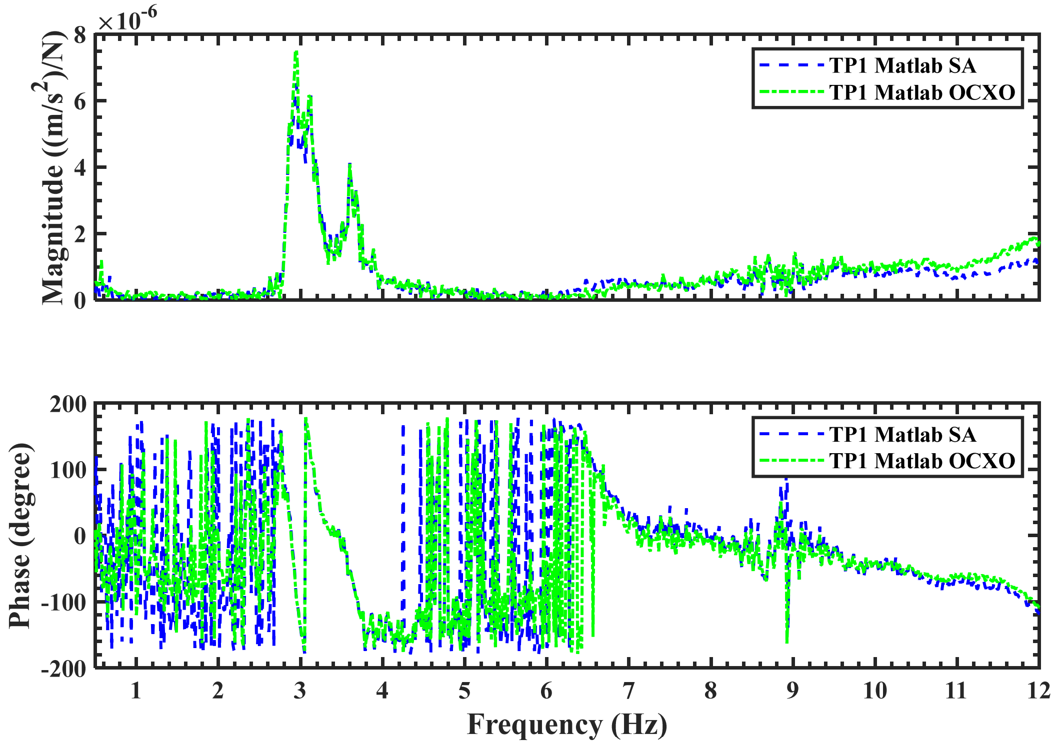


Figure 24: FRF transfer accelerance at TP1 between the excitation in the X-direction and response in the Y-direction (a) magnitude and (b) phase calculated by the spectrum analyser immediately (blue dashed line) and after return form the testing using OCXO data (green line). The FRF data quality is good and the two sets of SA- and OCXO-based FRF data are practically identical indicating the ability of the OCXO-based data acquisition system to reproduce high fidelity FRF data identical to the standard, tried and tested spectrum analyser system.

#### *4.6.3. Excitation in Y-direction*

After acquiring and quality-assuring raw data in the X-direction, the shakers were rotated by 90 degrees to excite the building in the Y-direction, see Figure 20b. A testing process identical to the X-direction was followed and similar good quality of FRF data were obtained. To support that, Figure 25a shows FRF point accelerances for the X- and Y-directions at TP1. They indicate that the X- and Y-direction excitations resulted in a logical complementary set of point accelerance FRFs demonstrating that the lowest modes of vibration have components in both orthogonal directions as expected considering the FE-calculated mode shapes (Figure 5). Figure 25b shows that the two FRF transfer accelerances between X and Y DOFs at TP1 look nominally identical, indicating a successful FRF reciprocity check ([7]).

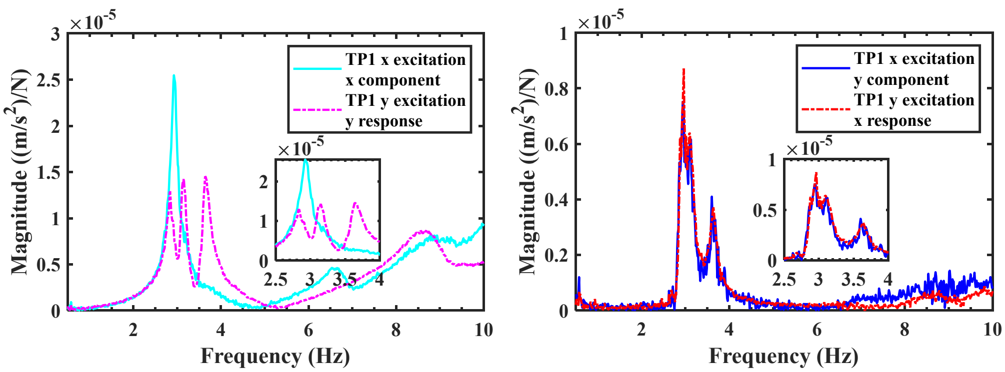


(a) Moduli of FRF point accelerances

(b) Moduli of FRF transfer accelerances

Figure 25: Comparison of FRFs at TP1 for shaker excitations in the X- and Y-directions. (a) are point accelerances. (b) are transfer accelerances between DOFs in X and Y directions at TP1.

### *4.6.4. Coherence function*

The coherence function is defined as the relationship between input and output signals. Two highly correlated signals have an ideal linear constant parameter proportion when the coherence function is equal to one. The quality of the FRF-based measurement and the presence of noise can both be evaluated using the coherence function as an indicator. The noise could enter the measurement if the coherence function is less than one but greater than zero, which refers to the non-linear proportion between the input and output signals. Alternatively, the output signal could be caused by the original and other inputs. If the coherence is zero, the input and output signals are completely independent of one another. Figure 26 shows the coherence function for X- and Y-directions at TP1. The clustering frequency ranges of 2-4 Hz, 5.5-6.5 Hz, and 7-12 Hz have coherence values that are almost close to 1 with strongly correlated input-output signals and have a tolerable amount of noise for the presentation of these modes. The range of 0-2 Hz and 4-5 Hz has a low coherence value due to uncorrelated relationships or no mode happened.

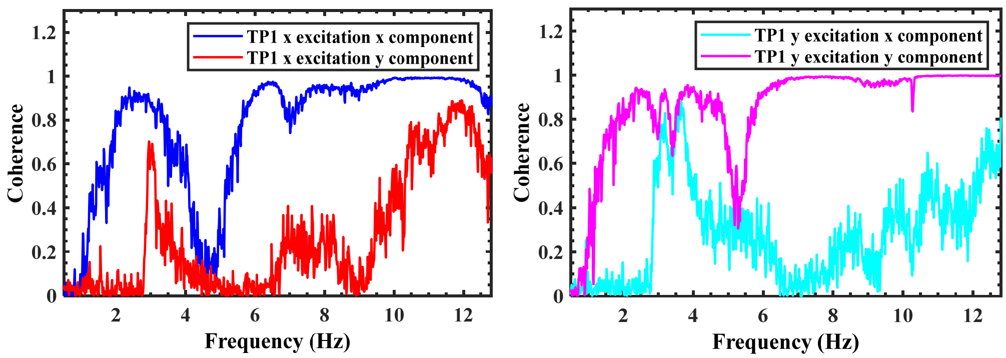


(a) Coherence function (b) Coherence function

Figure 26: Coherence function of input output signal at TP1 for shaker excitations in the X- and Y-directions. (a) X and Y responses related to X-direction excitation. (b) X and Y responses related to Y-direction excitation.

### *4.6.5. Static stiffness check*

By integrating twice the two measured FRF point accelerances, their corresponding FRF point receptances can be calculated ([14]). Figure 27 shows that the excellent quality of the FRF data enables an estimation of the static stiffness at TP1 using the horizontal part of point receptance FRF modulus plot before the rise of the curve towards the first resonant peak. The experimentally estimated static stiffnesses are: $k_{TP1,X,EXP} = 143$ MN/m and $k_{TP1,Y,EXP} = 123$ MN/m. These compare well with their counterparts for the pre-test FE model with values readily available during the testing: $k_{TP1,X,FE} = 170$ MN/m and $k_{TP1,Y,FE} = 150$ MN/m, indicating that the FE model is up to 22 % stiffer than the test structure at TP1. The right order of magnitude and a relatively small error further increased confidence in the test data.

This was a last quality assurance check indicating good FRF data despite the large size and normal operation (generating plenty of the extraneous noise) of the as-built structure.

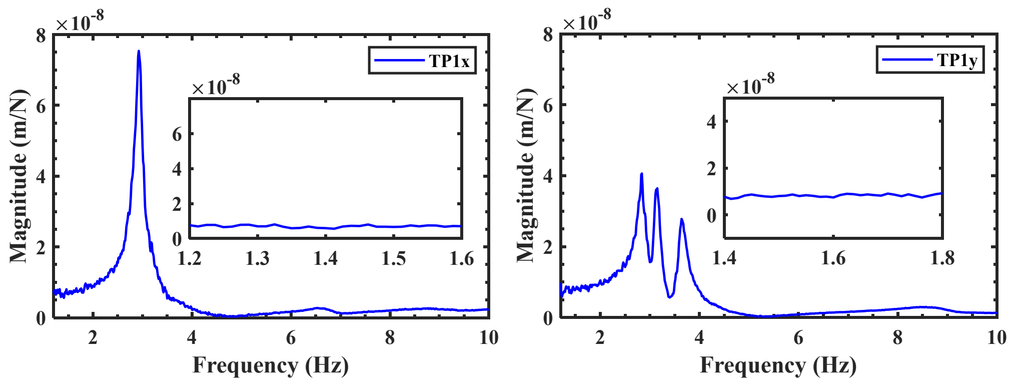


(a) X-direction modulus of FRF point receptance

(b) Y-direction modulus of FRF point receptance

Figure 27: FRF point receptances for TP1 in the (a) X-direction and (b) Y-direction.

## 5. Modal testing results

### *5.1. Modal analysis*

After the return to base, MATLAB code was used to process all of the data acquired using the OXCO-synchronised boxes yielding two columns of the FRF matrix measured. Therefore, it was possible to perform a multi-input multi-output (MIMO) curve-fitting procedure in which all FRFs are curve-fitted simultaneously ([14]). The multi-reference curve-fitting was done in the MEScope software [15] using the Complex Mode Indicator Function (CMIF) algorithm and two reference FRFs at TP1, corresponding to the DOFs in the X- and Y- directions, respectively. The good quality of the curve-fitting is demonstrated in Figure 28 with a clear indication that the two key point accelerance FRFs are well curve-fitted.

Finally, Figure 29 shows the estimated modal properties of this building. Despite the limited test grid, the modal properties in Figure 29 are logical and of exceptionally good quality. There are two clear clusters of modes: around 3-4 Hz and 7-12 Hz. As previously mentioned, by visual inspection of the FE-calculated modes, similar clustering of modes is also presented in the FE modelling (Figure 5). This observation further enhances confidence in the FRF-based modal testing results. Figure 30 also compares the experimental and FE models' natural frequencies, MAC values, and mode shapes before and after model updating. Again, the updated model's result obtained an acceptable match to the measurement. More specific information about the model updating may be found in the author's previous paper [8].

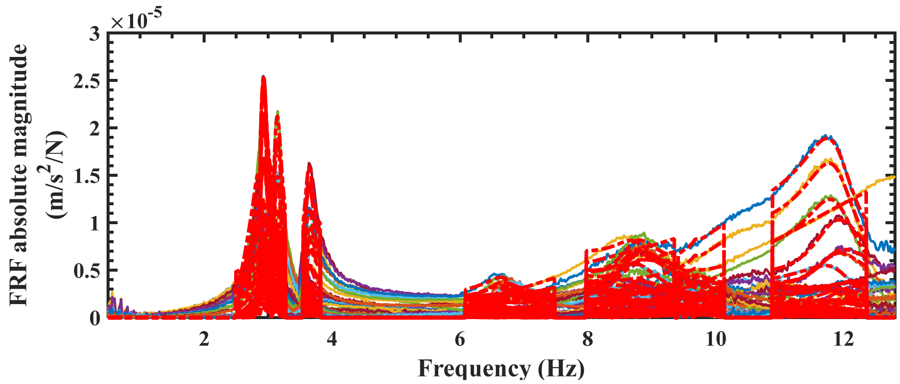


(a) Curve-fitting of moduli of all 52 FRFs

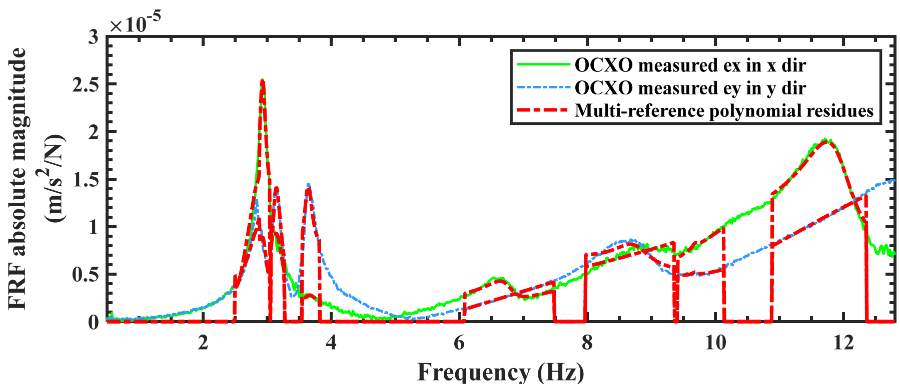


(b) Curve-fitting of moduli of two FRF point accelerances

Figure 28: Results of MIMO multi-reference curve-fitting with the estimated model represented by a dashed red trace plotted over the 52 (2 × 26) measured FRF moduli.

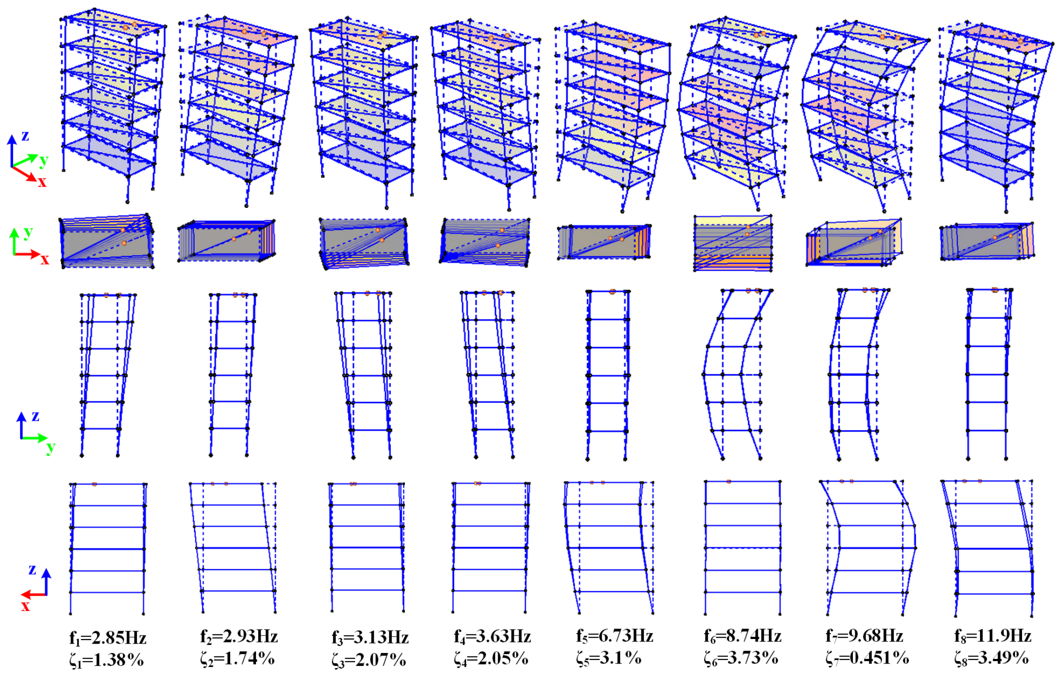


Figure 29: Estimated experimental modal properties using multi-reference FRF curve-fitting.

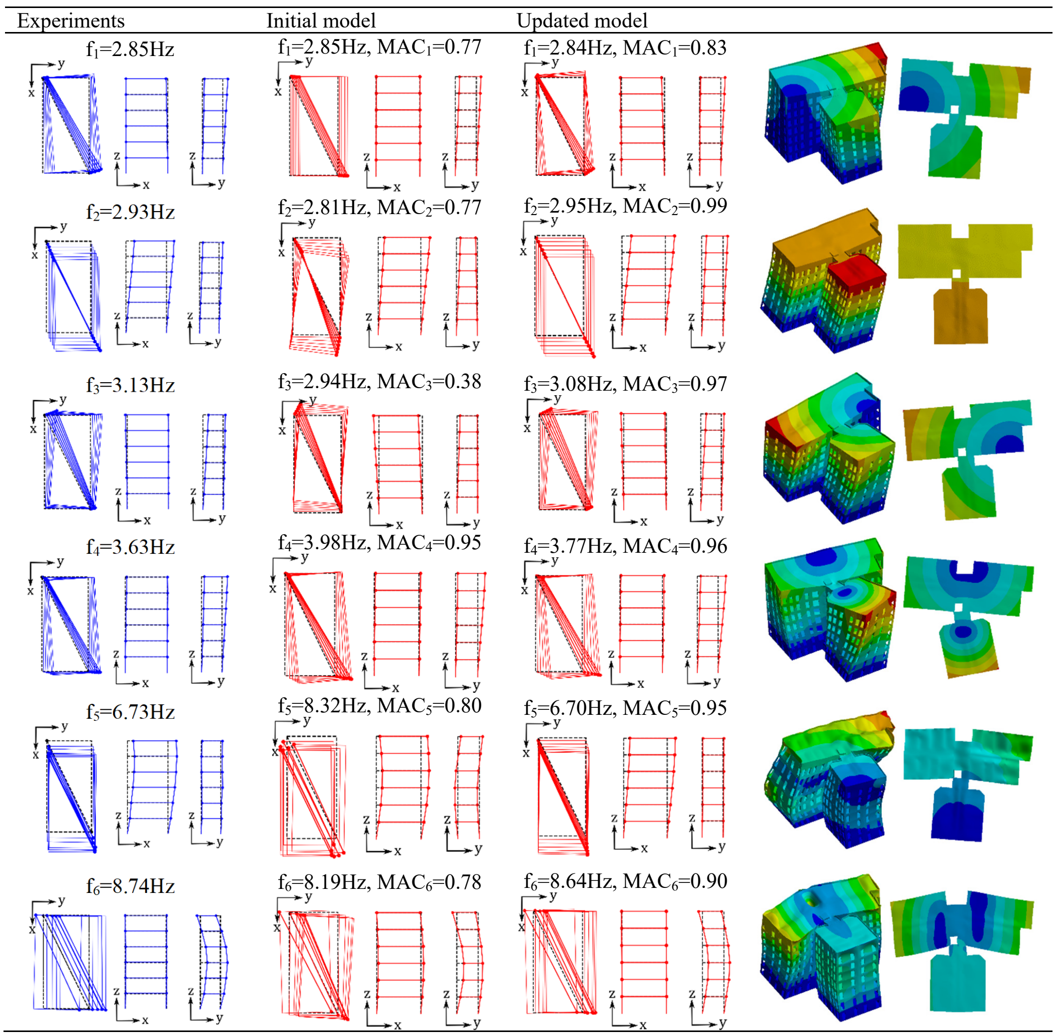


Figure 30: Graphical comparison of initial and updated model with experimental data (after [8]).

### 5.2. Evaluation of potential excitation level

Figure 31 shows the FRF magnitude plot driving in current and voltage modes of one APS shaker. The current drive at 1.5 Hz exhibited a clear resonant with a prominent peak. After 2 Hz, the platform may be steady with a constant output, but the voltage drive would not experience this kind of peak overshoot. Therefore, the voltage drive was selected in this horizontal excitation setup. Random excitation was used for the first test in the modal testing, with a driving voltage of 2 V per shaker. The first mode of the structure is 2.85 Hz, burying into the shaker's steady output dynamic frequency range. This might ensure that the shaker's driving force will be sufficient to excite the structure to the right level.

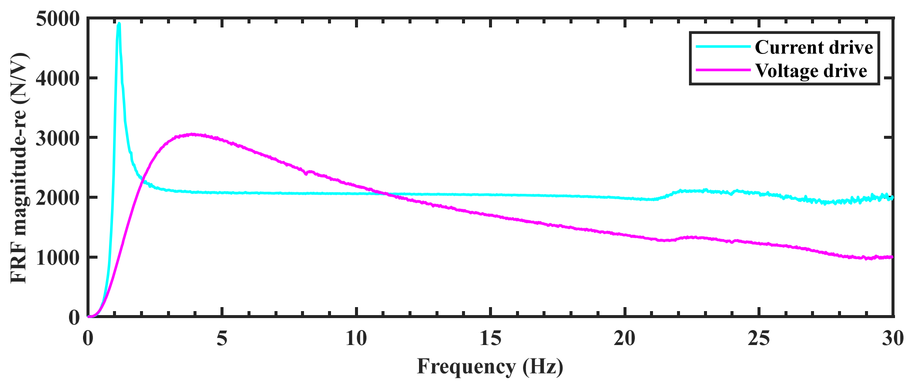


Figure 31: FRF magnitude plot of APS shaker driving in current and voltage modes.

Figure 32 shows a single APS shaker's excitation force time history, which had an amplitude of about 165 N root mean square (RMS). Otherwise, Figure 23a depicts the total excitation force, with an RMS amplitude of about 500 N needed to excite a 1300 tonne timber building.

A technical report from concrete society suggested the response calculation of low-frequency floor [16], the steady-state acceleration response at a position i in a single mode n of frequency $f_n$ at a given excitation frequency $hf_p$ can be calculated as follows:

$$a_{i,n}\left(hf_p\right) = \mu_{i,n}\mu_{j,n}\left(\frac{hf_p}{f_n}\right)^2 \frac{P_{j,h}}{M_n}\text{DMF} \tag{1}$$

where $hf_p$ is the harmonic excitation frequency. The harmonic excitation force of amplitude $P_{j,h}$ is applied at location $j$. $\mu_{j,n}$ is mode shape amplitude

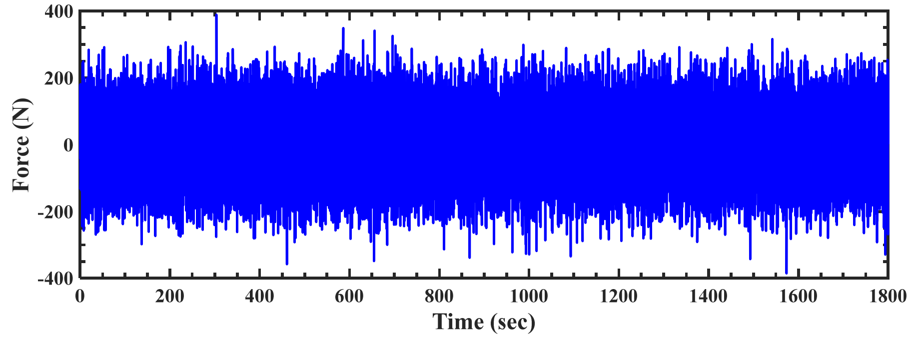


Figure 32: Single APS shaker random excitation force in the X-direction applied at TP1

at location $j$. $\mu_{i,n}$ is mode shape amplitude at location $i$. DMF is the dynamic magnification factor for steady-state harmonic response in the case of single mode, which could be given by:

$$\mathrm{DMF} = \frac{1}{\sqrt{\left[1 - \left(\frac{hf_p}{f_n}\right)^2\right]^2 + 2\zeta_n \left(\frac{hf_p}{f_n}\right)^2}} \tag{2}$$

where $\zeta_n$ is the viscous damping ratio for mode n. Taking the excitation point/location as a reference (TP1), the $\mu_{j,n}$ and $\mu_{i,n}$ could assume equal 1.

Additionally, the structure was excited with sinusoidal input using its resonance frequencies. Due to the input energy being concentrated at a single frequency, the sinusoidal input would produce a greater acceleration response than the random white noise signal. Figure 33 shows the three-run total input force time history of the first mode resonant frequency. The corresponding structural acceleration allowance level could be calculated using equations 1 and 2 and the modal parameters of the first mode, which is given by:

- The first resonant frequency: $f_1 = 2.85$ Hz,
  Harmonic excitation force of amplitude $P_{j,h}$ at TP1: $P_{1,1} = 770$ N,
  The first mode modal damping: $\zeta_1 = 1.38$ %,
  The first mode modal mass: $M_1$=1067296.729 kg, then
  Allowable steady-state acceleration level at TP1 of the first mode: $a_{1,1} = \frac{P_{1,1}}{M_1\sqrt{2\zeta_1}} = 0.043\,({}^{m}\!/_{s^2})$

The allowable acceleration level is the maximum acceptable root mean square (RMS) acceleration for a given fundamental frequency of a structure. Figure 34 displays the response at TP1 related to each run. The RMS acceleration value is around 0.0105 m/s$^2$, which is 4 times lower than the allowable acceleration level. From this point of view, the shaker excitation is sufficient to excite the structure and ensure an adequate level of shaking, not excessively high or low.

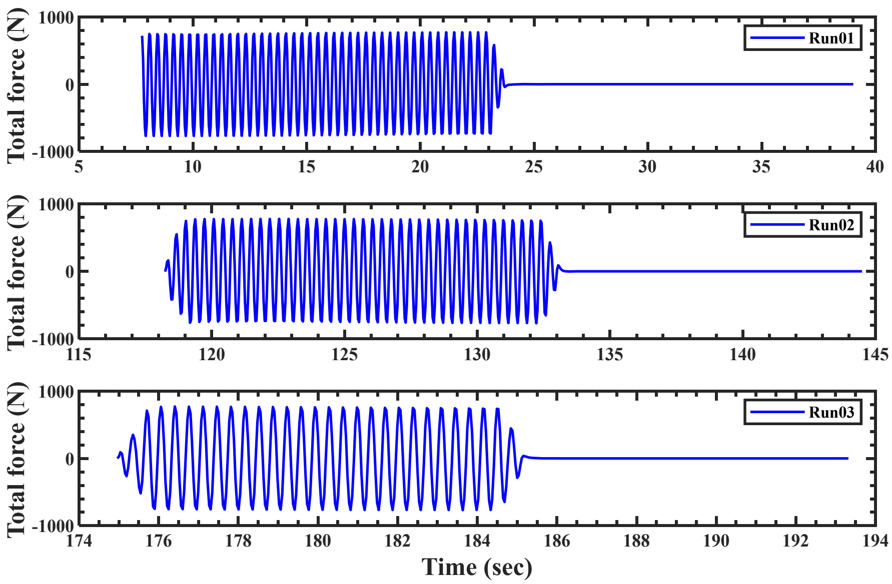


Figure 33: Total sinusoidal input force time history using the first resonant frequency.

Figure 34 shows three runs' total input sinusoidal force under the second resonant mode frequency. Similarly, the modal parameters of the second mode are used to calculate the allowable acceleration level, which is given by:

- The second resonant frequency: $f_2 = 2.93$ Hz,

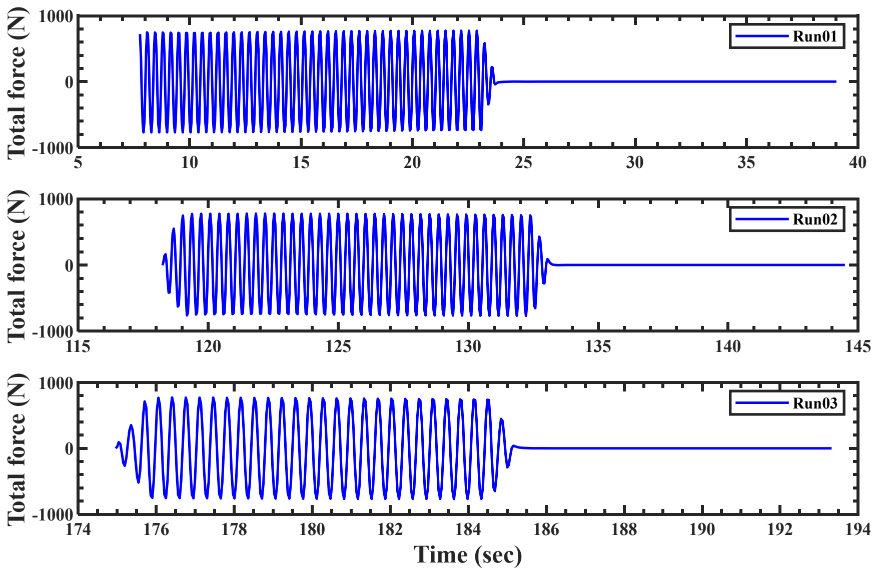


Harmonic excitation force of amplitude $P_{j,h}$ at TP1: $P_{1,2} = 813$ N, The second mode modal damping: $\zeta_2 = 1.74$ %, The second mode modal mass: $M_2 = 1524571.956$ kg, then Allowable steady-state acceleration level at TP1 of the second mode: $a_{1,2} = \frac{P_{1,2}}{M_2\sqrt{2}\zeta_2} = 0.029\,({}^{m}/{}_{s^2})$

This configuration setting of the APS electromagnetic dynamic shaker could be customised to fit various low-frequency buildings and structures. The adjustment requires adding a mass source to the shaker as a horizontal reaction mass system, as shown in Figure 35. Table 1 also illustrates an idea of the lowest frequency connected to the shaker's addition of mass bars (each mass bar weighs 24.8 kg). The goal is to ensure the force can supply sufficient excitation and full steady energy to drive the shaker. Therefore, it was necessary to know the first mode resonant frequency in advance and change the shaker's setup accordingly. The number of shakers could also be employed to regulate the level of the total input force, ensuring that the force suitably excites the structure. Figure 36 shows the extra information related to a high-rise building in Norway to apply this methodology to capture the structural dynamics.

## 6. Operational modal analysis of ambient vibration testing (AVT)

The ambient vibration testing could be conducted to capture dynamic response under service load (i.e., wind-induced excitation). However, the

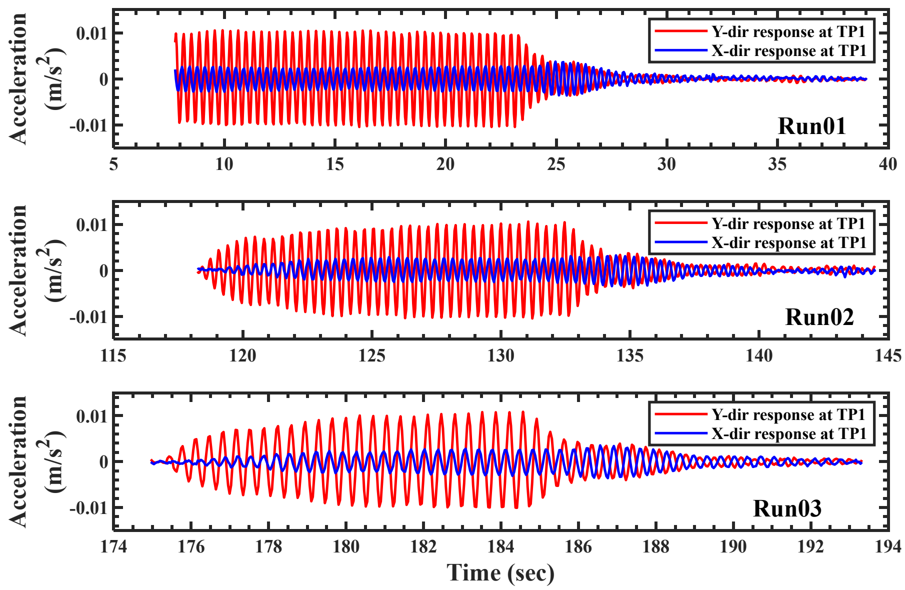


Figure 34: Acceleration response at TP1 under the first resonant frequency sinusoidal excitation.


Figure 35: Horizontal reaction mass system with APS shaker.

| Quantity of mass bars | 0 | 2 | 4 | 6 | 8 | 10 | 12 | 14 | 16 | 18 | 20 | 22 |
|---|---|---|---|---|---|---|---|---|---|---|---|---|
| Lowest frequency for rated force (Hz) | 1.11 | 0.9 | 0.83 | 0.8 | 0.69 | 0.64 | 0.6 | 0.6 | 0.55 | 0.52 | 0.5 | 0.48 |

Table 1: Horizontal reaction mass system extra mass versus lowest rate frequency


Figure 36: Photo of the application of APS shaker with horizontal reaction mass system.

amount of sway produced by wind is mostly small amplitude/movement than the dynamic exciters created. Additionally, the low-frequency dynamic characteristics have always been easily generated by the service load, whereas the high-frequency dynamic characteristics are difficult to get using the OMA method.

The x and y directional acceleration time histories of each test point channel under ambient loading are shown in Figure 37. The measurement duration of the ambient data was around an hour. It can be seen that wind excitation caused some considerable amplitude/vibration to occur at specific times, particularly around 3000, 4000, and 4500 s. The response during rest time remained at the usual vibration level.

As illustrated in Figure 38, the acceleration raw time history data could be used to obtain the power spectral density function (PSD). The low-frequency dynamics could readily be captured using the peak-picking technique (e.g., under 6 Hz for Yoker Building); however, high-frequency modes could not be excited by the ambient loading since there was not enough energy (e.g., over 10 Hz for Yoker Building). The measured result using FRF (see Figure 28) demonstrated better high-frequency dynamic response capturing. Additionally, the frequency range of roughly 6 to 8 Hz in the ambient OMA result could not provide a good compromise to the FRF-based measurement.

The identified modes of a structure can be effectively visualised using a stabilisation diagram of the covariance-driven subspace stochastic identification (SSI-COV) results. The stabilisation diagram provides a graphical

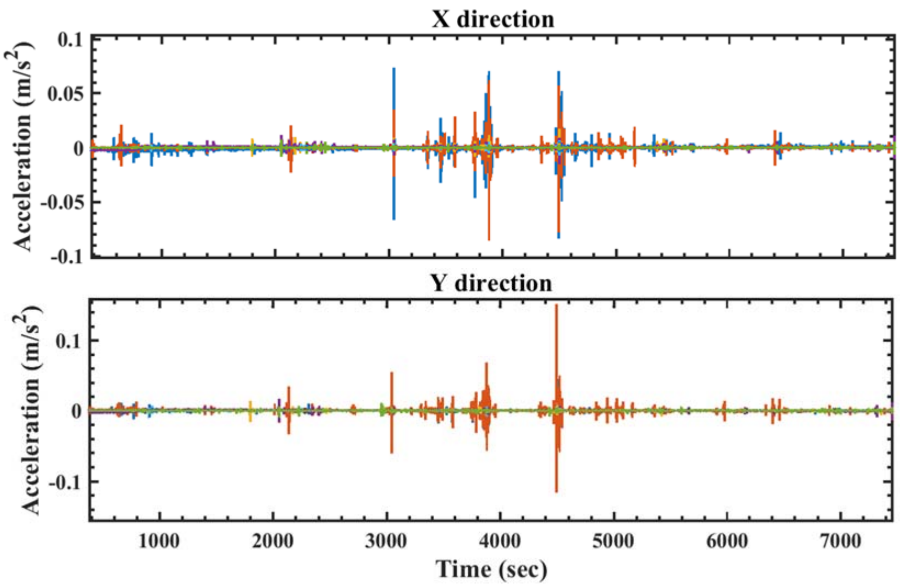


Figure 37: One-hour acceleration time history of ambient vibration testing in X- and Y-directions

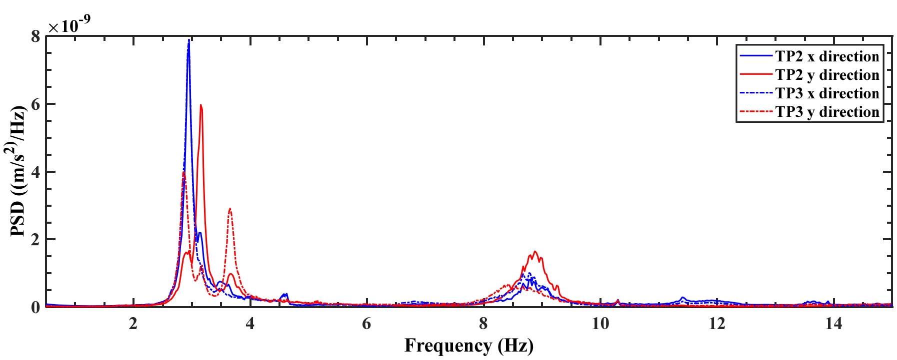


Figure 38: Power spectral density function (PSD) of the ambient vibration testing data.

representation of a system's poles (modes) at different model orders when identifying the modal parameters (see Figure 15 left-hand side y-axis). The blue circle symbol represents the stable poles, which occurred between 2.5-4 Hz and 8.5-9 Hz.

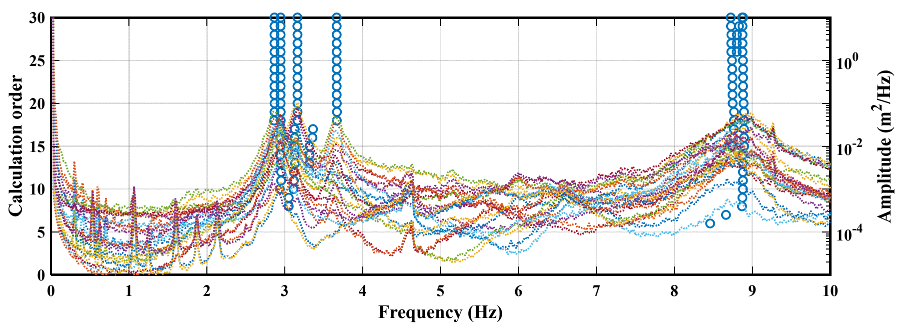


Figure 39: Stabilisation diagram

The estimated modal characteristics of the structure under ambient excitation are shown in Figure 40. The environmental loading efficiently aroused the low-frequency range 2-5 Hz modes, and stability verification from Figure 39 also provided assurance that these range estimated modes are logical. However, comparing the damping values estimation from output-only OMA and FRF-based measurement, the output-only result is usually higher than FRF curve-fitting. Furthermore, compared to FRF-based measurement (see Figure 28), the frequency range 6-9 Hz modes are hardly found since they could not have been significantly caused by the ambient loading (see Figure 38). Additionally, the stability checking in Figure 39 is inevitably shown that 6-7 Hz mode is not a reliable mode via ambient OMA.

Looking at the estimated modal properties, notable advantages of the FRF-based modal testing relative to the standard output-only AVT are:

(a) Ability to identify well higher modes of vibration which is practically not possible with AVT relying on environmental loading (e.g., wind), which simply does not have the energy in the 7-12 Hz region and cannot excite modes in that frequency range. AVT-based methods to estimate modal properties of as-built operational buildings almost never measure higher order bending modes of vibration of multi-storey buildings as reliably as demonstrated here.

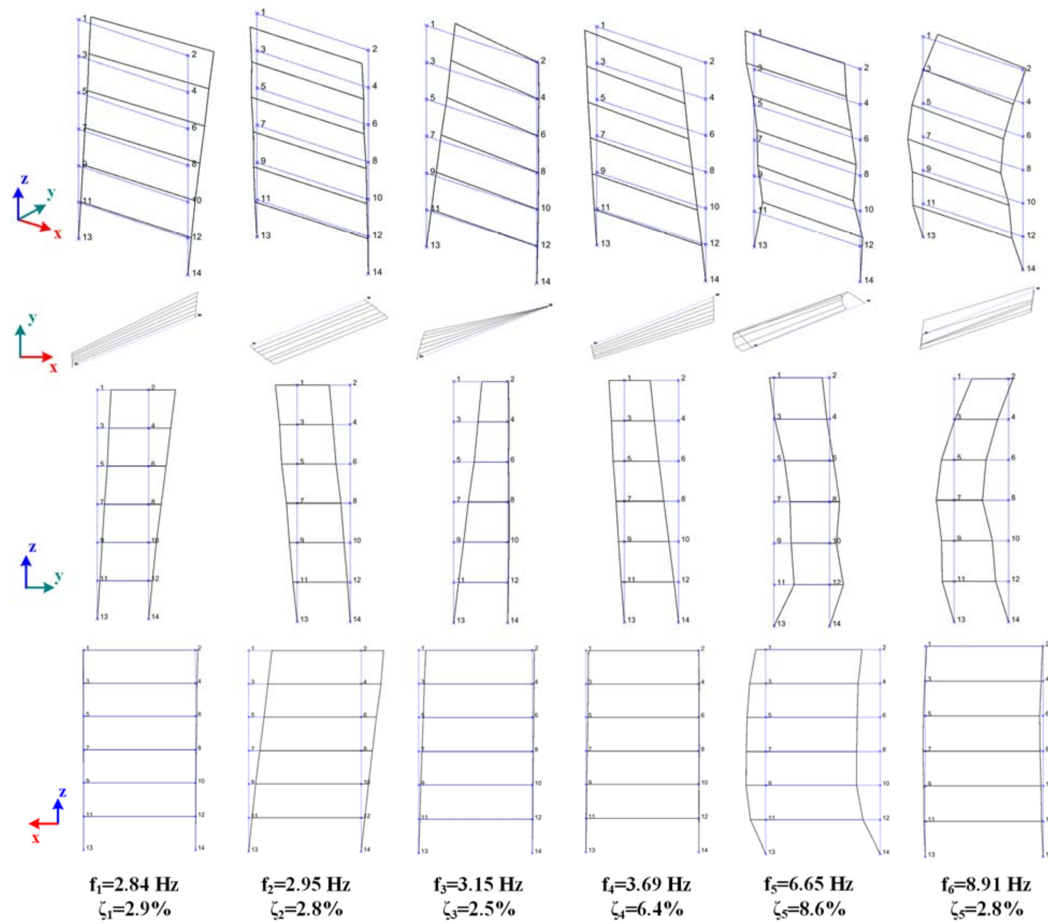


Figure 40: Estimated modal properties using ambient vibration testing data

(b) In multi-storey timber buildings in particular, which tend to have relatively high fundamental frequency compared with really tall standard steel and/or concrete multi-storey buildings, these higher modes may be useful to estimate the as-built stiffness of connection joints by FE model updating. This is because the such high frequency and clean bending modes engage structural joints much more than the fundamental modes of vibration. This study is beyond the scope of this paper and is presented elsewhere ([8]).

(c) Damping values are notably higher in the cluster of higher modes (apart from mode 7 outlier value) compared with the cluster of the lower modes. It is not clear what is causing this and is speculated there that it could also be a feature of the greater engagement of timber joints which do not contribute only to the structural stiffness but also to its damping. This feature merits further investigation.

## 7. Conclusions

This paper presented a novel input-output FRF-based MT of a multi-storey CLT residential building with 42 occupied flats in normal operation. The key observations and conclusions are listed below.

- The testing was a success, although it was carried out exceptionally fast within only a single working day but following 6 months of preparations. The testing lasted only 10 h from arrival to the site and starting the instrumentation from scratch to leaving the site completely.

- The testing was carried out using purposely built OCXO-synchronised data loggers, which did not require connecting signal wires running through the building. This even though every of the six-floor levels was monitored at least at four horizontal DOFs, yielding excellent descriptions of the mode shapes over 26 DOFs throughout the whole building.

- The limited common area of the building corridor leading to individual flats at each level, over which the instrumentation was allowed, was sufficient to measure key modal features of the building structure. This was helped and confirmed by the key features of the pre-test FE model, which correlated well with the modal data from the limited set of measurement points.

- Random excitation 0-12 Hz by three synchronously running APS400 shakers with a total force of only 500 N RMS was able to excite the whole 1300-tonne building sufficiently to yield good quality FRFs between the excitation DOF at TP1 at the top of the building and response DOFs throughout the building. Key to this was the low-noise OXCO-based data acquisition system coupled with excellent ultra-sensitive DC accelerometers.

- A QA process was followed throughout the testing ensuring the best quality modal data for not less than eight modes of vibration. This is a significant number of quality modes compared to typical AVT output-only methods used on operational multi-storey buildings. Preliminary FE analysis was carried out to inform the modal testing and provide confidence in the measured FRF and modal data during the intense 10h of field testing.

- In the low-frequency region of the measured FRFs a useful feature has been the ability to estimate experimentally the horizontal static stiffness at the top of the building, a feature not seen before for tall structures. It was shown that the preliminary best practice FE model was over-predicting the static stiffness by only up to 22 % of the measured values.

- In the high-frequency region of the measured FRFs higher order modes of vibration were identified in the region 7-12 Hz yielding in general modal damping ratios of over 3 %. This damping ratio is quite high for a multi-storey building. These high-order mode shapes could further be used to investigate sources of stiffness and damping in timber joints in a manner not done before. This is because such higher modes of vibration of a timber building have not been experimentally measured in the past in the 7-12 Hz region, which is quite typical for novel multi-storey CLT buildings. Although beyond the scope of this paper, this could be a consequence of the higher modes bending more and engaging more the CLT connections than the lower-order modes. This greater engagement, in turn, generates more modal damping in the higher-order modes. This is an important feature that needs further investigation and could be exploited in new designs of CLT structures.

## 8. Acknowledgement

The support of ERA-NET Cofund Forest Value (for the DynaTTB project https://www.dynattb.com) and the corresponding funding bodies (Ministry of Education, Science and Sport of the Republic of Slovenia and UK Forestry Commission). Special thanks go to Smith and Wallwork Ltd at Cambridge, UK who are designers of the Yoker building for providing the required design information and helping secure access to the structure.

## References

[1] K. C. S. Kwok, Human perception and tolerance of wind-induced building motion. Chapter 12 in Advanced Structural Engineering, Edited by Y. Tamura and A. Kareem., Springer, 2013.

[2] A. E. Aktan, J. M. W. Brownjohn, Structural identification: Opportunities and challenges, ASCE Journal of Structural Engineering (10) (2013) 1639–1647.

[3] N. Satake, K. Suda, T. Arakawa, A. Sasaki, Y. Tamura., Damping evaluation using full-scale data of buildings in japan, ASCE Journal of Structural Engineering (4) (2003) 440–477.

[4] S.-K. Au, Operational Modal Analysis - Modeling, Bayesian Inference, Uncertainty Laws, Springer, 2017.

[5] C. Rainieri, G. Fabbrocino, Operational Modal Analysis of Civil Engineering Structures, Springer, 2014.

[6] W. K. Ao, A. Pavic, Discovering the dynamic properties of civil structures with frf-based and wirelessly synchronised, distributed ocxo high-precision data loggers, In: IMAC-XXXIX Congress, Orlando, FL, USA, 8-11 February.

[7] D. T. A. DTA, The dynamic test agency handbook, Tech. rep., Dynamic Testing Agency-NAFEMS (1994).

[8] B. Kurent, B. Brank, W. K. Ao, Model updating of seven-storey cross laminated timber building designed on frequency-response-functions-based modal testing, Structure and Infrastructure Engineering (1).

[9] Stora Enso, European technical assesment ETA-14/0349 of 03.06.2019, Tech. rep., Austrian institute of construction engineering (2019).

[10] J. M. W. Brownjohn, S.-K. Au, Y. Zhu, Z. Sun, B. Li, J. Bassitt, E. Hudson, H. Sun, Bayesian operational modal analysis of jiangyin yangtze river bridge, Mechanical Systems and Signal Processing (1).

[11] W. K. Ao, A. Pavic, Frf-based modal testing of horizontally swaying structures using ocxo synchronized wireless accelerometers for simultaneous force and vibration responses measurements, In: EURODYN 2020 XI International Conference on Structural Dynamics, Athens, Greece, 23-25 November.

[12] Honeywell International, Inc., Q-flex qa-750 accelerometer, Tech. rep., Honeywell International, Inc. Defense and Space Electronic Systems Redmond (2020).

[13] Japan Aviation Electronics Industry, Ltd., Mems ja-70sa accelerometers, Tech. rep., Japan Aviation Electronics Industry, Ltd. (2021).

[14] D. Ewins, Modal Testing Theory and Practice, Research Studies Press LTD, 1984.

[15] V. T. Inc, ME'SCOPE, Vibrant Technology Inc.: www.vibetech.com, March 2020.

[16] Report of a Concrete Society Working Party, Tr 43 post-tensioned concrete floors - design handbook 2nd edition, Tech. rep., Japan Aviation Electronics Industry, Ltd. (2005).